Research Article

Development of an *Ex Vivo* Aneurysm Model for Vascular Device Testing

Noemi Vanerio[1,2], *Marco Stijnen*[1], *Bas A. J. M. de Mol*[2] and *Linda M. Kock*[1,3]

[1]LifeTec Group BV, Eindhoven, The Netherlands; [2]Department of Cardiothoracic Surgery and Cardiovascular Sciences, Amsterdam University Medical Center, Amsterdam, The Netherlands; [3]Department of Biomedical Engineering, Eindhoven University of Technology, Eindhoven, The Netherlands

Abstract

An *ex vivo* aneurysm model that closely resembles the *in vivo* situation can provide an important tool to test therapeutic approaches while avoiding animal experimentation. The model should mimic a variety of conditions, such as *in vivo* hemodynamics and native arterial structure and characteristics. The aim of this study was to develop an *ex vivo* aneurysm model by stiffening vessel walls to be used to assess treatment strategies. Porcine carotid arteries from slaughterhouse animals were used to evaluate the acute effect of different concentrations of Rose Bengal on vessel distensibility. Rose Bengal is a sono-sensitive compound that is activated by several ultrasound frequencies, resulting in stiffening of the treated arteries; the most effective combination of concentration and frequency was determined. In a pulsatile *ex vivo* vascular bioreactor, treated and control porcine carotid arteries were subjected to physiological conditions for 10 days. Treated arteries showed increased mean pressure and decreased pulsatility compared to controls. Changes in vessel morphology and a significant increase of distal diameter were observed in the treated arteries but not in the controls. Histology revealed distal dissection-like lesions and proximal aneurysm-like structure in the treated arteries. Finally, a stent graft was deployed and cultured in one treated artery, demonstrating the feasibility of testing endovascular devices in the model. In conclusion, we developed an *ex vivo* model reproducing the onset of aneurysm formation. This represents a promising tool for early stage device testing, thereby reducing the need for animal studies.

1 Introduction

Abdominal aortic aneurysm (AAA) is a life-threatening and often asymptomatic cardiovascular disease consisting of an abnormal dilation of the aorta owing to vessel wall weakening, which develops until rupture. The prevalence of AAA is ≈ 5% in men and ≈ 1% in women older than 60 years (Golledge and Norman, 2011); rupture carries a 90% overall mortality (Giugliano et al., 2018; Upchurch and Criado, 2009).

The etiology and pathogenesis of aneurysms are poorly understood. It seems that aneurysm formation is associated with a significant increase in stiffness of the arterial wall compared to healthy tissue in both AAA (He and Roach, 1994; MacSweeney et al., 1992; Sonesson et al., 1997; Vande Geest et al., 2006) and cerebral aneurysms (Robertson et al., 2015). Mechanical properties of the arterial wall, such as stiffness, depend on extracellular matrix composition, particularly on the amount, orientation, and crosslinks of elastin and collagen fibers (Gasser et al., 2012). In fact, reduction and degradation of elastin in end-stage AAA have been shown to stimulate aneurysm development (Campa et al., 1987; Carmo et al., 2002; Isenburg et al., 2007), and therefore loss of elastin is believed to be the main characteristic of aneurysms.

In the last years, aneurysm development has been increasingly linked to impaired collagen homeostasis (Lindeman et al., 2010). However, studies based on the analysis of collagen content in AAA tissue showed discordant results, observing a decrease (McGee et al., 1991), an increase (He and Roach, 1994; Rizzo et al., 1989) or no changes (Gandhi et al., 1994) in collagen content. Collagen crosslinking has been shown to be increased in AAA (Carmo et al., 2002; Lindeman et al., 2010; Wågsäter et al., 2013), and alterations in collagen microarchitecture in AAA and Marfan's syndrome tissue resulted in tissue mechanical failure (Lindeman et al., 2010). However, the exact role of collagen in aneurysm pathophysiology and whether the loss of elastin function or collagen crosslinking or their combination triggers the pathology is still unknown.

To optimize treatment and better understand aneurysm pathophysiology, several *in vivo* animal models have been developed

Received June 25, 2019; Accepted October 21, 2019;
Epub October 23, 2019; © The Authors, 2019.

ALTEX 37(1), 110-120. doi:10.14573/altex.1906253

Correspondence: Linda M. Kock, PhD,
LifeTec Group BV, Kennedyplein 10-11,
5611 ZS Eindhoven, The Netherlands
(l.kock@lifetecgroup.com)

over the years to mimic aneurysm onset, progression and rupture. Patelis et al. (2017) and Lysgaard Poulsen et al. (2016) reviewed the main *in vivo* models of AAA, underlining the high number of animal models used for this purpose.

In rodent animal models, aneurysms are induced by using porcine pancreatic elastase (Mao et al., 2015; Nuki et al., 2009), calcium chloride infusion (Isenburg et al., 2007), implantation of xenografts, angiotensin II infusion in knockout mice (Trachet et al., 2016) or by creating transgenic models (Lysgaard Poulsen et al., 2016). These models have good reproducibility, elastase leads to fast dilatation, calcium chloride and angiotensin II models induce aneurysms without arterectomy, and formation of an intraluminal thrombus is commonly obtained in the xenograft models. However, all these models require major surgery and are technically difficult in addition to being time-consuming, costly, and unsuitable for device testing because of the rodent vessels' different size and morphology (Lysgaard Poulsen et al., 2016). Therefore, these models are mainly used to investigate the pathological mechanisms.

For interventional testing, non-rodent larger animal models were introduced. In these models, aneurysms are mainly induced chemically, with elastase, collagenase (or combinations of both) (Czerski et al., 2013) or calcium chloride, or mechanically by using grafts or patches (Lysgaard Poulsen et al., 2016). In chemically induced models, aneurysm formation is achieved in terms of elastin disruption and diameter dilatation only when a combination of elastase, collagenase and angioplasty is used. Long-term studies have not yet been reported. In the mechanical aneurysm models, anatomical characteristics can be reproduced, and some pathological similarities to aneurysms in patients were found, but no further enlargement of the aneurysm can be obtained.

In addition to the limitations of the rodent and non-rodent animal models mentioned above, the use of *in vivo* animal models implies ethical issues, time- and money-consuming protocols, high complexity of the model, and poor controllability of the experiments. Considering the limitations of *in vivo* models and the 3R principle, *ex vivo* aneurysm models using slaughterhouse tissue could be a valuable alternative that could reduce *in vivo* animal models (Lysgaard Poulsen et al., 2016; Patelis et al., 2017), overcoming limitations and disadvantages of *in vivo* studies while including biological response and physiological environment, which are limited or absent in *in vitro* testing. Moreover, *ex vivo* aneurysm models could provide a tool to study aneurysms at early phases of the disease, which is otherwise not possible since tissue is mostly only harvested after aneurysm rupture.

Recently, different *ex vivo* aneurysm models have been described. In one of these models, PTFE grafts were dilated to create an aneurysmal scaffold seeded with stromal vascular fraction cells and cultured in a bioreactor for 14 days (Touroo and Williams, 2012). The development of a tissue-engineered aneurysm model was supported by the formation of a layer of smooth muscle cells (SMCs). This model could be used as a testing platform for endovascular devices, however the lack of native tissue is a limitation because of the absence of physiological tissue composition, structure, and biomechanical properties. Another study focused on the phenotype of SMCs isolated from porcine carotid arteries that were treated with collagenase and elastase and cultured in a steady-flow bioreactor for 12 days (Riches et al., 2013). The phenotype of the isolated SMCs showed changes comparable to end-stage AAA samples in terms of rhomboid morphology, increased spread area, senescence, and impaired proliferation. This approach allows SMC dysfunction studies, especially focusing on early stage aneurysm development. On the other hand, absence of physiological pulsatile hemodynamics and non-significant diameter changes were reported.

Based on the limitations of the other *ex vivo* models, we consider that an *ex vivo* aneurysm model that closely resembles the *in vivo* situation and conditions, such as *in vivo* hemodynamics and native blood vessel structure and characteristics, is still missing. Therefore, the aim of this study was to develop a novel *ex vivo* aneurysm model based on stiffening and subsequent culturing of porcine carotid arteries. It has been shown that the pathogenesis and etiology of aneurysms is only minimally dependent on their location within the vasculature (Tanweer et al., 2014). Due to the similarities in structure and characteristics between the aortic and carotid wall and because carotid arteries are considered good models of AAA in other *ex vivo* (Riches et al., 2013) and *in vivo* (Patelis et al., 2017) experiments, carotid arteries were used in this study.

Stiffening of biological tissues can be induced experimentally by exploiting photochemical-based processes using, for example, Rose Bengal (RB), a xanthene dye that can be activated by green light or by ultrasound (Bekesi et al., 2017; Cherfan et al., 2013; Salinas et al., 2017; Xu et al., 2015). Upon activation, RB can create covalent bonding of structural proteins such as cross-links in collagen molecules, leading to tissue stiffening. Treatment of *ex vivo* carotid arteries with RB activated by ultrasound is assessed in this study with regard to its ability to induce arterial wall stiffening and, ultimately, aneurysm formation. First, the acute effect of different concentrations of RB in combination with different ultrasound frequencies on the mechanical properties of native porcine carotid arteries was evaluated in order to select the best combination. Second, achievement of aneurysm formation was evaluated in terms of long-term response of carotid arteries to RB-ultrasound treatment in the pulsatile *ex vivo* vascular bioreactor. Finally, to demonstrate the feasibility of testing endovascular devices in the platform and to assess whether the device has influence on the further development of the aneurysm, a pilot study was performed in which a stent graft was implanted in a treated carotid artery cultured in the *ex vivo* vascular bioreactor.

2 Animals, materials and methods

All porcine common carotid arteries used in the experiments were obtained from Dutch Landrace pigs, 5-7 months old, weighing 100-110 kg, from a local slaughterhouse, following the routine slaughtering procedure. Each carotid artery was obtained from a different pig.

Tab. 1: Experimental groups for testing the acute effect of Rose Bengal-ultrasound treatment on arterial distensibility
Combinations of RB concentrations and US frequencies.

		Ultrasound (US) frequency		
		0 MHz	**3.5 MHz**	**7.5 MHz**
RB	0 %	untreated	RB0.0US3.5 (control)	RB0.0US7.5 (control)
	0.1 %	RB0.1US0 (control)	RB0.1US3.5	RB0.1US7.5
	1 %	RB1.0US0 (control)	RB1.0US3.5	RB1.0US7.5

2.1 Acute effect of RB-ultrasound treatment on arterial distensibility

2.1.1 Carotid artery preparation

In the slaughterhouse, the carotid arteries were immediately flushed after dissection with cold phosphate-buffered saline (PBS, Sigma-Aldrich, Zwijndrecht, The Netherlands at 4°C) to remove blood. They were subsequently stored in PBS on ice until their arrival in the laboratory within 1 h after slaughter. Upon arrival, the carotid arteries were trimmed to remove the surrounding connective tissue while submerged in cold PBS.

2.1.2 Experimental groups

Prepared carotid arteries ($n \geq 3$ per group) were divided into 8 groups (Tab. 1). Each artery underwent distensibility testing within 3 h of isolation and was then treated with RB and/or ultrasound. Distensibility testing was repeated within 1 h on the treated arteries to evaluate the effect of the RB-ultrasound treatment. In each group, a different combination of RB concentration and ultrasound (US) frequency was used (Tab. 1). The chosen concentrations of RB have been previously reported as non-cytotoxic in photochemical tissue bonding applications (Barton et al., 2012; Xu et al., 2015). The clinically most used and easily available ultrasound frequencies were selected for testing.

2.1.3 RB-ultrasound treatment

Carotid arteries were mounted proximally and distally in a support chamber and filled with RB solution (0.1% or 1% w/v RB in PBS; Rose Bengal sodium salt, dye content 95%, Sigma-Aldrich, Zwijndrecht, The Netherlands) using a 10 mL syringe without a needle (BD Plastipak™, Fisher Scientific, Landsmeer, The Netherlands). RB solution was allowed to diffuse into the vessel wall for 3 min before the vessel underwent sonication treatment for 2 min, using an ultrasound machine (SSD-2000, Aloka, Tokyo, Japan) equipped with a 3.5 or 7.5 MHz probe.

2.1.4 Distensibility testing protocol

Mechanical properties of untreated and treated porcine carotid arteries were evaluated and compared in terms of distensibility. Each artery was mounted on connectors in a dedicated setup and stretched to 150%, which is the physiological pre-stretch of porcine carotid arteries *in vivo* (Boekhoven et al., 2014). The artery was maintained at room temperature in a PBS bath during the test. Fixed volumes of PBS were injected with a syringe at 0.1 mL/s until a pressure of around 160 mmHg was reached. Pressure values inside the artery were recorded by a pressure transducer (BD P10EZ, Becton Dickinson, Sandy, Utah, USA) and the signal was transmitted to a PC through a pressure amplifier (Picas, Peekel Instruments BV, Rotterdam, The Netherlands) and a breakout box (NI BNC-2090, National Instruments, Austin, Texas, USA).

At the end of the test on the untreated artery, RB-ultrasound treatment was performed on the vessel while mounted in the vessel chamber of the setup. The distensibility test was then repeated on the treated carotid artery following the same protocol.

2.1.5 Data analysis and statistics

Distensibility of the arteries was analyzed by comparing the normalized change in volume (compared to initial volume of fluid present in the artery) and the measured hydrostatic pressure. Distensibility values represent the slope of the normalized volume versus the hydrostatic pressure curve for physiological pressure values at or above 90 mmHg. Data is expressed as mean ± SEM. Two-tailed paired Student's t-test was used to analyze distensibility differences between untreated and treated arteries, and $P < 0.05$ was considered statistically significant.

2.2 Long-term response of carotid arteries to RB-ultrasound treatment

2.2.1 Carotid artery preparation

In the slaughterhouse, harvested porcine common carotid arteries ($n = 8$) were directly flushed with ice-cold sterile modified Krebs solution (Krebs-Henseleit solution supplemented with 10^{-1} mM papaverine (Sigma Aldrich, St. Louis, MO, USA), 0.05 mM 2-mercaptoethanol (Gibco™, LifeTechnologies, Bleiswijk, The Netherlands), 2% antibiotic penicillin-streptomycin (10,000 U/mL, Gibco™), 0.6% antimycotic amphotericin B (0.75 ng/mL, Gibco™)) and transported immediately to the lab on ice in sterile jars containing modified Krebs solution. In a laminar flow hood, vessels were gently trimmed to remove excess connective tissue, minimizing damage to the endothelium, and segments of 6 cm length were cut while submerged in fresh, cold, sterile modified Krebs solution. Half of the prepared vessels ($n = 4$) were treated with sterile-filtered (0.22 µm, Fisher Scientific, Landsmeer, The Netherlands) 1% w/v RB solution and 3.5 MHz ultrasound frequency before being placed in the bioreactor. Previous results showed that this combination is the most effective to stiffen the arterial tissue.

2.2.2 Experimental setup

Porcine carotid arteries (n = 8) were cultured in a pulsatile *ex vivo* vascular bioreactor for 10 days (day 0: start of culture, day 9: end of culture) under physiological hemodynamics at a temperature of 38°C, 100% humidity, and 5% CO_2 (Vanerio et al., 2019a). The arteries were divided into 2 experimental groups: control group (n = 4), consisting of untreated arteries, and treated group (n = 4), consisting of arteries treated with 1% RB solution and 3.5 MHz ultrasound frequency. During culture, hemodynamic parameters were measured continuously and acquired hourly, while ultrasound imaging was performed daily.

2.2.3 Culture protocol in *ex vivo* vascular bioreactor

A previously described custom developed *ex vivo* vascular bioreactor was used (Vanerio et al., 2019a). The bioreactor consists of a reservoir chamber, in which fresh medium is stored, an in-house developed circulation pump, which pumps the fresh medium from the reservoir into a first compliance chamber, which dampens pressure and flow curves, a vessel culture chamber, in which an artery can be placed, and a *Windkessel* model (variable resistance-compliance chamber-variable resistance) to replicate the vascular impedance of the systemic circulation, which is connected back to the reservoir.

Briefly, under a laminar flow hood, the artery was mounted on connectors and positioned in the vessel culture chamber equipped with an ultrasound window for vessel imaging. Culture medium was pumped from the reservoir into the lumen of the artery by the in-house developed pump, and pulsatile physiological hemodynamics were set using the compliance chambers and adjustable resistances. Connection between the reservoir and the vessel culture chamber allowed for external perfusion of the artery. A medium refreshment circuit provided 2 mL/min of fresh medium.

All arteries were cultured in Dulbecco's Modified Eagle's Medium containing 1 g/L D-glucose, 25 mM HEPES, 1mM pyruvate, 4mM L-glutamine (Gibco™ DMEM, low glucose, pyruvate, HEPES, Gibco, LifeTechnologies, Bleiswijk, The Netherlands) supplemented with 50 µM 2-mercaptoethanol (2-Mercaptoethanol (50 mM) Gibco™), 10% fetal bovine serum (Gibco™), 1% antibiotic penicillin-streptomycin (Penicillin-Streptomycin (10,000 U/mL) Gibco™), antimycotic amphotericin B (0.75 ng/mL, Amphotericin B, Gibco™), vascular endothelial growth factor (VEGF 2.5 ng/mL, PeproTech Inc., Rocky Hill, NJ, USA) and xanthan gum (0.66 g/L, Fisher Scientific, Landsmeer, The Netherlands) to mimic blood-like viscosity.

Upon start of the culture, a physiological longitudinal prestretch of 150% was applied to the arteries. After a warm-up phase of 3 h, in which the pressure was gradually increased to 120/80 mmHg, the flow rate was set to achieve a physiological shear stress value of 2.4 Pa (Vanerio et al., 2019a).

2.2.4 Data analyses

Hemodynamics

Pressure values were measured up- and downstream of the vessel using pressure transducers (RT2000 system, Argon Medical Devices Netherlands B.V.), and the flow rate was measured at the inlet of the vessel using an ultrasonic flow sensor (Sono TT and OEM Flow Measurement Board, Em-tec GmbH, Finning, Germany).

Ultrasound imaging

An ultrasound machine (Esaote Picus Pro with arterial analyzer Art.Lab, Esaote Europe, The Netherlands) equipped with a linear probe (7.5 MHz acquisition frequency) was used to perform ultrasound imaging. Diameter estimation was achieved upon determination of inner and outer borders of the artery with in-house developed software (based on Loizou et al., 2009). Shape, straightness and intima-media-adventitia layer structure were qualitatively analyzed in post-processed ultrasound images.

Histology

At the end of the culture, rings of the proximal and distal part of the cultured vessels (n = 4 per group) were cut, embedded in Tissue-Tek O.C.T. Compound (Sakura Finetek USA Inc, Torrance, California, USA) and snap frozen in isopentane solution (2-Methylbutane, Sigma Aldrich, St. Louis, MO, USA). 5 µm-thick sections were cut with a cryostat (SLEE MNT, SLEE medical GmbH, Mainz, Germany), mounted on a glass slide and stained for collagen and elastin, using a commercially available kit (Modified Verhoeff Van Gieson Elastic Stain Kit, Cat. HT25A Sigma Aldrich, St. Louis, MO, USA). All sections were examined under an optical microscope (Eclipse TE300, Nikon) at a magnification of 4x, and digital pictures (CMEX-3 Digital Microscope Camera DC.3000c, Euromex Microscopen BV, Arnhem, The Netherlands) were taken.

2.2.5 Statistics

To calculate the diameter change, diameter values were normalized to diameter at day 1, which is the timepoint at which the vasoconstriction due to the harvesting procedure is recovered; therefore, the diameter value is comparable to the *in vivo* condition. Diameter changes were expressed as mean ± SEM. Two-way ANOVA analysis was used to evaluate the influence of time and treatment on diameter. Post-hoc comparisons using Bonferroni correction were used to determine significant differences between groups per timepoint. $P < 0.05$ was considered statistically significant.

2.3 Device assessment – pilot study

A pilot study was performed to assess the feasibility of testing endovascular devices in the *ex vivo* aneurysm model. A porcine carotid artery (n = 1) was cultured in the *ex vivo* vascular bioreactor following the protocol above after treatment with 1% RB solution and 3.5 MHz ultrasound frequency. After the artery was cultured for 6 days, a 5 mm x 12 mm stent graft (Jostent GraftMaster®, Abbott Vascular Inc., Santa Clara, California, USA) was delivered over a guidewire and deployed at 16 atm in the distal segment of the cultured carotid artery under ultrasound guidance. The artery was then further cultured for 4 days to reach a total of 10 days of culture. During culture, hemodynamics data were acquired hourly, and ultrasound imaging was performed daily. Histological analyses were performed at the end of the culture.

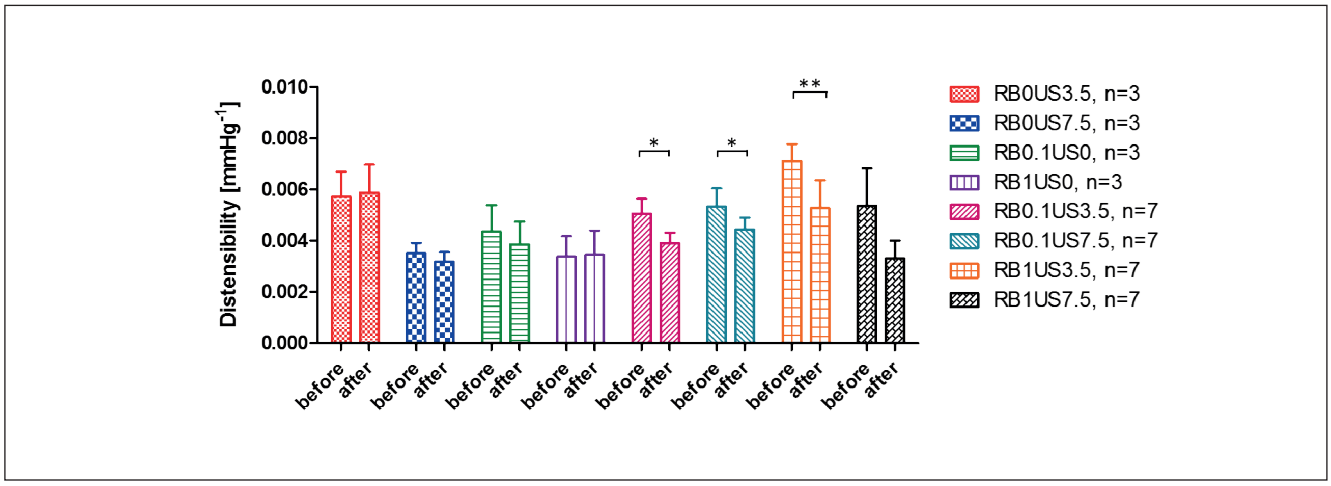

Fig. 1: Distensibility values comparing arteries treated with combinations of different concentrations of Rose Bengal (RB: 0, 0.1, 1%) and ultrasound frequencies (US: 0, 3.5, 7.5 MHz)

Control groups treated with either RB or ultrasound show no statistically significant difference of distensibility between arteries before and after the treatment. A statistically significant decrease of distensibility is observed in arteries after treatment with both RB and US, with the exception of RB1US7.5. Values are displayed as mean ±SEM; *$p < 0.05$; **$p < 0.001$.

3 Results

3.1 Effect of RB-ultrasound treatment on arterial distensibility

Distensibility of porcine carotid arteries was compared before and after treatment with RB and ultrasound by analyzing the slope of the normalized volume in the artery versus the hydrostatic pressure curve above 90 mmHg (Fig. 1). Treatment with either only RB without ultrasound activation (RB0.1US0, RB1US0) or with only ultrasound without RB infusion (RB0US3.5, RB0US7.5) did not result in a significant change in distensibility compared to the untreated situation. The distensibility of arteries treated with both RB and ultrasound was significantly decreased compared to the distensibility of the same arteries before treatment, except for the combination of 1% RB and 7.5 MHz ultrasound, which was not statistically significant. To compare the different groups, the distensibility ratio defined as ratio between the distensibility before the treatment and the distensibility after the treatment was calculated. The distensibility ratio of the RB1US3.5 group was the highest, although not statistically significantly different from the other groups (data not shown), and was used in further experiments.

3.2 Long-term response of carotid arteries to RB-ultrasound treatment

Treated porcine carotid arteries (n = 4, RB 1% US 3.5 MHz) and untreated control arteries (n = 4) were cultured in the *ex vivo* vascular bioreactor for 10 days and compared in terms of hemodynamics, vessel geometry, wall structure and composition. All arteries showed the same trend within their group except for one of the treated arteries, which is presented separately at the end of the paragraph because of the divergent response that was observed.

For the other treated arteries (n = 3) and the untreated controls (n = 4), one cycle (660 s) of pressure curves at the start and at the end of the culture is shown in Figure 2. At day 2, the pressure curves of the control and treated groups overlap in the pulsatile physiological range of 120/80 mmHg (Fig. 2A). On the contrary, at day 9 the pressure curve of the treated group shows an increased mean pressure and reduced pulsatility, defined as difference between the maximum and the minimum pressure values, compared to the untreated control group (Fig. 2B), although the pressure curves remain in the physiological range.

Geometry change of the vessels was evaluated during culture in terms of diameter change of proximal and distal segments of control (n = 4) and treated (n = 3) arteries (Fig. 3). The proximal segments show a statistically significant increase in diameter over time in both treated and control arteries ($p < 0.0001$). Moreover, the diameter of treated arteries is significantly increased compared to control arteries at days 3, 5 and 8, reaching a value of 1.36 (Fig. 3A). In the distal segments (Fig. 3B), an increase in diameters is observed over time in both treated and control groups ($p < 0.0001$). The diameter increase of treated arteries is significantly greater (reaching 2.15) compared to the untreated controls (reaching 1.26) at all timepoints ($p < 0.0001$).

Vessel wall structure and composition were analyzed by daily ultrasound imaging, and histology was performed at the end of the culture on proximal and distal segments. Figure 4 shows ultrasound and histology images of a representative untreated control (n = 4, Fig. 4A) and a treated (n = 3, Fig. 4B) artery after being cultured for 10 days.

Elastin and collagen Verhoeff-Van Gieson (VVG) staining of untreated control arteries shows that the vessel wall presents a compact structure and physiological extracellular matrix in both distal (Fig. 4A-a) and proximal segments (Fig. 4A-b). Rectilinear morphology and physiological vessel wall structure of control arteries is also visible in ultrasound imaging (Fig. 4A-c). In

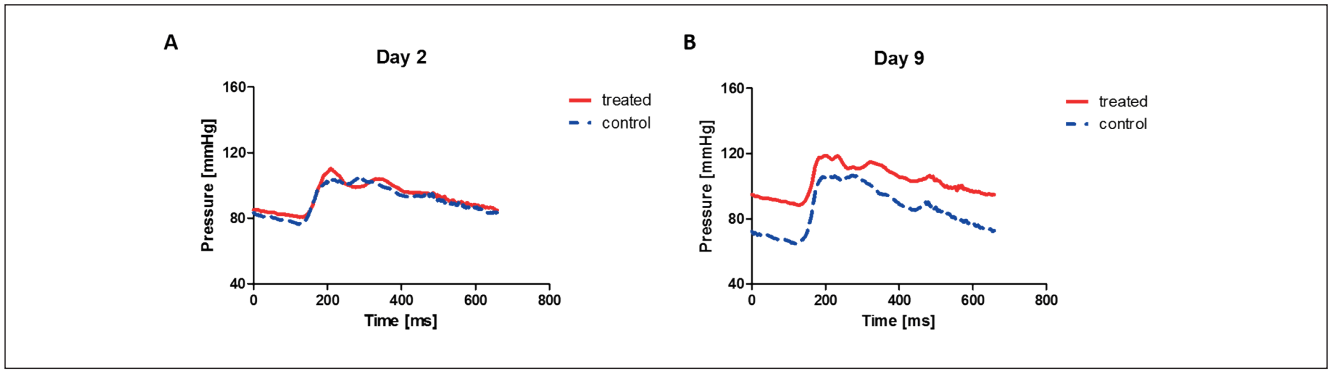

Fig. 2: Pressure curves at day 2 and 9 measured in porcine carotid arteries cultured in the *ex vivo* vascular bioreactor, comparing control group (n = 4) and treated group (n = 3)

(A) No differences are noticeable at day 2 between controls and treated arteries. (B) Increase of mean pressure is shown in treated carotids compared to controls at day 9.

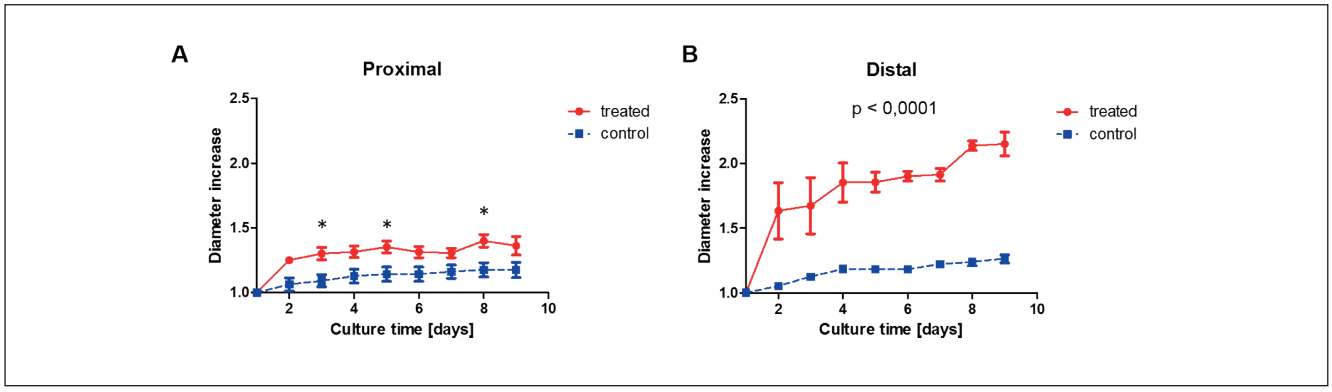

Fig. 3: Diameter change of proximal and distal porcine carotid arteries during culture in the *ex vivo* vascular bioreactor, comparing control group (n = 4) and treated group (n = 3)

(A) Slight difference in increase of proximal diameter in treated arteries compared to controls over time. Statistically significant increase in diameter over time for both control and treated arteries ($p < 0.0001$). (B) Statistically significant difference in increase of distal diameter in treated arteries compared to controls at all timepoints and over time in both control and treated arteries ($p < 0.0001$). Values are displayed as mean ±SEM.

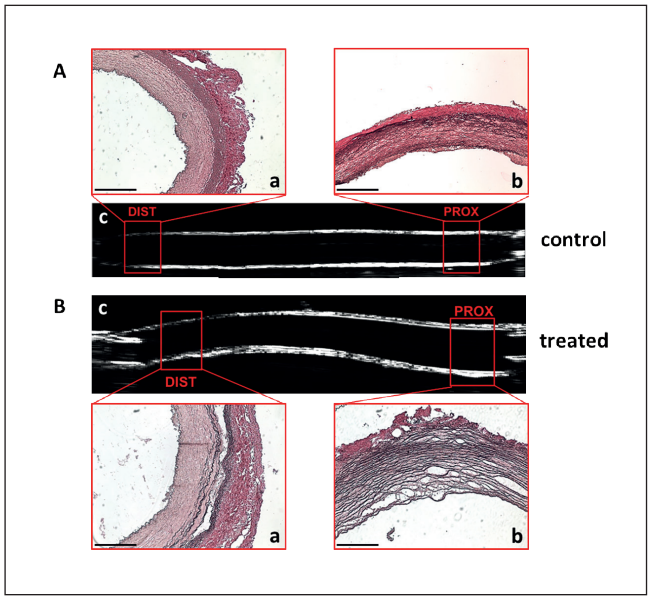

Fig. 4: Histology and ultrasound images of control and treated vessels at day 9 of culture in the *ex vivo* vascular bioreactor

(A) Untreated control arteries: Verhoeff-Van Gieson (VVG) staining shows physiological structure in both (a) distal and (b) proximal segments; (c) physiological vessel morphology and structure are visible in ultrasound imaging. (B) Treated arteries: VVG staining shows (a) separation of the vessel wall layers in the distal segments and (b) loose wall structure in the proximal segments; (c) changes in vessel morphology are shown by ultrasound imaging. VVG: Collagen fibers are stained red; elastin fibers are stained black; scale bar: 500 μm.

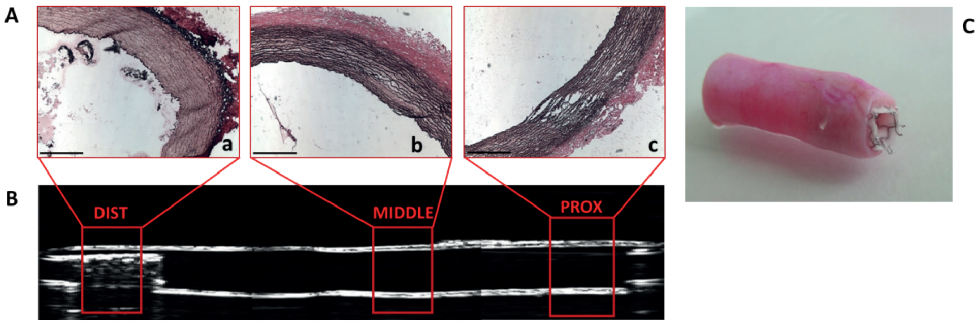

Fig. 5: Stent graft implanted in the *ex vivo* aneurysm model
(A) VVG staining shows compact structure and stent fragments in distal (a), physiological structure in middle (b), and damage of the extracellular matrix in proximal (c) segments. (B) Physiological morphology and stent graft implanted in the distal segment, visible with ultrasound imaging at day 9. (C) Carotid artery with implanted stent graft at the end of the culture. VVG: Collagen fibers are stained red; elastin fibers are stained black; scale bar: 500 μm.

contrast, in treated arteries, VVG staining showed separation of the vessel wall layers, disorganization of the elastin fibers in the distal segments (Fig. 4B-a), and moderate disruption of the extracellular matrix, resulting in loose structure with visible spaces between elastin fibers in the proximal segments (Fig. 4B-b). Ultrasound images of the treated vessels display a curvature of the vessel and increased wall thickness (Fig. 4B-c).

A divergent response was observed in one of the treated porcine carotid arteries compared to all other arteries within the same experimental group and to controls, summarized in Figure S1[1]. In terms of hemodynamics, at the end of the culture the pressure curve of the divergent, treated artery showed a high increase of mean pressure, absence of pulsatility, and values of pressure above the physiological range of 120/80 mmHg (Fig. S1A-b[1]) compared to the other treated and untreated arteries. Vessel geometry assessment revealed a large increase in diameter in both distal (Fig. S1B-a[1]) and proximal segments (Fig. S1B-b[1]). Over time, the vessel lost its straight morphology, and separation of the vessel wall layers occurred, leading to bulge development (Fig. S1C[1]). VVG staining showed loose wall structure with visible spaces in the distal segment (Fig. S1D-a[1]). Massive disruption of the extracellular matrix and bulge formation was observed close to the proximal segment (Fig. S1D-b[1]). Tissue growth and moderate disruption of the extracellular matrix was visible in the proximal segment (Fig. S1D-c[1]).

3.3 Device assessment – pilot study

A stent graft was successfully implanted in the distal part of a treated carotid artery at day 6 and cultured for 4 days in the *ex vivo* vascular bioreactor. Elastin and collagen VVG staining shows compact and overall regular extracellular matrix structure and fragments of the stent graft in the distal segment (Fig. 5A-a), compact and regular tissue structure in the middle segment (Fig. 5A-b), and presence of empty spaces and elastin disruption in the extracellular matrix of the proximal segment (Fig. 5A-c). At day 9, ultrasound imaging displays the presence of the stent graft in the distal part, predominantly straight morphology and physiological vessel wall layer structure (Fig. 5B). In Figure 5C, the stent graft implanted in the carotid artery is shown. No macroscopic response of the vessel to the stent was noted.

4 Discussion

In this study, we developed a novel *ex vivo* aneurysm-like model by wall stiffening of cultured native porcine carotid arteries with sono-activated RB.

First, the immediate effect of different combinations of sono-activated RB on the mechanical properties of porcine carotid arteries was investigated. The distensibility values of the tested carotid arteries were comparable to previously reported values (Roy et al., 2005). A possible explanation of the observed differences in distensibility of the vessels among the groups before treatment is ascribed to inter-subject variability. A statistically significant decrease of distensibility was observed only in arteries that were treated with both RB and ultrasound. To our knowledge, this is the first study showing that sono-activated RB can be used to stiffen biological tissues. This method could be further explored for applications where photo-activation is not possible, for example, for *in situ* collagen crosslinking of deep tissue that cannot be reached by light non-invasively.

A similar effect was previously established using RB in combination with photo-activation, for example in photochemical tissue bonding applications (Cherfan et al., 2013; Lauto et

[1] doi:10.14573/altex.1906253s

al., 2010; O'Neill et al., 2007; Vanerio et al., 2019b). In photochemical tissue bonding, the reaction between RB and green light causes covalent bonding of structural proteins, leading to crosslinking of collagen molecules. In our case, sono-activation, instead of photo-activation, was proposed to avoid the use of green light sources, which are costly, more invasive, and require safety measures (Vanerio et al., 2019b). Our finding supports the hypothesis that photo- and sono-activation of RB induce similar reactions and mechanisms, eventually leading to similar stiffening outcomes. Although the precise mechanism of interaction between ultrasound and sono-sensitizers (e.g., RB) is unknown, other studies have suggested that cavitation caused by ultrasound induces chemical activation of sono-sensitizers, leading to free radical formation (Hiraoka et al., 2006; Nakonechny et al., 2013). Free radicals can react with amino acids, which can trigger crosslinking of collagen fibers, similar to what is observed in RB photoactivation. The lack of change in distensibility when one of the parameters (ultrasound or RB) is absent demonstrates that sono-activation and subsequent stiffening take place only when both stimuli are present. Lower RB concentrations seem to lead to a lesser distensibility decrease, which could be explained by having less RB in the vessel wall available for collagen crosslinking.

The combination RB1US3.5 was selected for the long-term culturing studies because it showed the most significant decrease of distensibility. It is not clear why the combination RB1US7.5 showed a non-significant decrease of distensibility. Since a higher US frequency is characterized by lower tissue penetration depth, this may have led to only partial activation of RB and therefore to less collagen crosslinking, resulting in a lesser decrease of distensibility. To test this hypothesis, quantification of collagen crosslinking needs to be performed.

In a next step, porcine carotid arteries were treated with sono-activated RB and subsequently cultured for 10 days in a vascular bioreactor. At the end of the culture, treated arteries showed a slightly higher mean pressure and lower pulsatility compared to controls, which was very pronounced in the divergent treated artery. This increase of mean pressure could be caused by a narrowing of the lumen of the tubes distally because of accumulation of detached cells or because of an increase of medium viscosity due to the possible secretum of the SMCs, although no blockage was observed. The decrease of pulsatility in the treated vessels can be considered a consequence of dilation of the vessels as, at a similar flow rate, the relative volume increase in the vessel during a single stroke contributes less to the total artery volume when the artery is already dilated. The ratio between the volume of the single stroke and the maximum artery volume is lower for higher artery volume, resulting in smoothening of the pressure curves.

The main distinctive characteristic of aneurysms is arterial dilation, which is considered to be aneurysmal when the artery diameter reaches 150% of the original diameter (Johnston et al., 1991; Nordon et al., 2011). In our untreated control vessels, a small increase in diameter, below 150%, was observed over time, which is probably caused by adaptation of the vessel to the new environment. Treated vessels showed increases in diameter exceeding 150%, especially in distal segments, already after 3 days of culture. In the divergent vessel, both proximal and distal diameter increases reached values of 200% and almost 300% for proximal and distal segments, respectively.

The aneurysm-like pathological appearance of the treated arteries is supported by ultrasound imaging and histological findings. Untreated control vessels showed physiological morphology while treated vessels showed curved morphology, probably due to extracellular matrix damage, which can lead to elongation and subsequent curvature. Elastin and collagen play a role in retaining tissue structure, and therefore alterations in their networks can lead to changes in the morphology. The pronounced s-shaped morphology of the divergent vessel visible in the ultrasound images could be due to buckling because of the high pressure values in the artery. Moreover, a noticeable bulging with delamination of the layers resembling dissection and aneurysm-like lesions *in vivo* was observed in the same vessel. Nevertheless, ultrasound images of carotid arteries cultured in the *ex vivo* vascular bioreactor cannot directly be translated and compared to ultrasound images taken *in vivo* because *in vivo* the arteries are surrounded by tissue, which limits the displacement or the curvature of the artery during the progression of the pathology, while in *ex vivo* systems, where no surrounding tissue is present, displacement and curvature can occur.

Elastin and collagen staining confirmed the ultrasound evidence by showing delamination of vessel wall layers distally and loose extracellular matrix structure in the proximal segments of the treated vessels. Histology of the cultured treated arteries presented several similarities to *in vivo* human and animal aneurysmal tissue. The observed distal separation of vessel wall layers can be related to dissection lesions in humans and animals (Chen et al., 2009). The proximal loose structure of the extracellular matrix with numerous lacunae may reveal disruption, fragmentation and degeneration of elastin fibers as observed in aneurysms and dissections in *in vivo* animal models (Isenburg et al., 2007; Li et al., 2016; Ren et al., 2016) and human biopsies (Chen et al., 2009). In the divergent treated vessel presenting bulge formation, extracellular matrix corresponding with the bulging segment was greatly disrupted. A clear difference that is noticeable when comparing *in vivo* aneurysm and dissection histology with treated arteries is the absence of a thrombus due to the fact that no blood is included in our *ex vivo* model.

The stiffening treatment was applied to the entire vessel, leading to a significant increase of the distal diameter and in the divergent case to severe enlargement of both proximal and distal diameters. In all treated vessels, histological analyses showed differences in aneurysm and dissection-like characteristics between proximal and distal segments. It is known that mechanical properties, extracellular matrix composition, and passive behavior of carotid arteries differ when comparing proximal and distal segments (García et al., 2012; Sokolis et al., 2011). We speculate that the reason why aneurysm-like lesions are located in the proximal segments is related to the elastic nature of the segment, while dissection-like lesions are located mostly in the distal parts due to the muscular nature of that part. However, the specific influence of the different vessel segments on pathol-

ogy progression is unclear; specifically, it is unknown whether this influence can be ascribed mainly to the passive viscoelastic mechanical properties or to the active vasomotor behavior of the carotid arteries. This point could be investigated by testing treated vessels with different vasodilators and vasoconstrictors to isolate the contribution of the passive and active properties of the vessels.

We speculate that the treated vessel showing divergent behavior might have been in a later stage of pathology progression compared to the other treated vessels, for example owing to a faster response to treatment. In fact, the increase of diameter and mean pressure and the decrease of pulsatility in the other treated arteries show an intermediate behavior between untreated controls and the divergent vessel. Moreover, the degradation of the extracellular matrix, which is visible in the treated vessels in terms of the presence of lacunae, is exacerbated in the divergent vessel. These observations support the hypothesis that the divergent vessel developed the pathology faster. Further experiments will be performed to assess whether this divergent behavior is possibly due to inter-subject variability.

A direct comparison of our outcomes with previous *ex vivo* aneurysm models cannot be performed. In the model described by Touroo and Williams (2012), no native tissue was used with the limitation of lack of real tissue structure. Moreover, dilation was created artificially in the ePTFE graft. In the model used by Riches et al. (2013), although damage to the extracellular matrix is shown, the *ex vivo* model was focused on SMC phenotype in early stage aneurysms, therefore the histological findings are not comparable. No ultrasound assessment was performed and dilation of the native vessels was not achieved, underlining the difference between our model and the other approaches.

A limitation of the present study is the use of FBS in the culture medium to provide proteins and growth factors in order to preserve expression of endothelial cell markers. The use of FBS raises ethical concerns because of its harvesting and collection. To overcome this limitation, we are currently looking into chemically-defined serum-free medium compositions in order to replace the use of FBS.

Currently, no blood is included in the circulation and therefore blood cells do not contribute to aneurysm development. This reveals that the pathological modifications that were observed in our model are due solely to the stiffening and not to blood cells (e.g., inflammatory cells), which are, however, believed to play a major role in aneurysm pathogenesis (Upchurch and Criado, 2009). For this reason, this model provides an interesting method to explore the specific contribution of stiffening, inflammation, and other factors to aneurysm pathogenesis and pathophysiology. To investigate this further and approach the *in vivo* situation more closely, it might be interesting to investigate the combination of the effect of stiffening and an inflammatory contribution by, for example, adding circulating blood cells to the culture medium. In fact, in separate studies not described in this paper, we included white blood cells (e.g., monocytes) in the *ex vivo* vascular bioreactor and found that the presence of circulating monocytes significantly improved the healing process in the intimal layer after denudation compared to vessels cultured without monocytes (unpublished data). Although the replacement of the culture medium with blood in the system could be interesting to investigate thrombus formation, applications like aneurysms coiling, and to be able to better compare histological results to *in vivo* data, this would require the use of anticoagulants, which does not represent a completely physiological condition since, for example, they affect the endothelial layer.

The feasibility of assessing endovascular devices in our *ex vivo* aneurysm-like model was demonstrated in a pilot study. The *ex vivo* vascular bioreactor proved suitable for sterile insertion, deployment and culture of a stent graft in a native vessel. The procedure was easier to perform than it would have been in an animal and allowed daily analysis, which is usually not possible in an animal. The sample showed a slower aneurysm progression compared to RB-ultrasound treated arteries without a stent graft. These outcomes provide the first experience of testing a medical device in an *ex vivo* pathological model, bringing *ex vivo* models closer to real clinical settings and possibly leading to a reduction of *in vivo* animal studies. More studies will be needed to let the true pathology evolve further before being able to study these interventions. This pilot study paves the way for testing devices for longer time periods, which would allow a better comparison with *in vivo* human and animal data and assessing novel devices and treatment approaches, such as pharmacokinetics and scaffold-cell interaction in *in situ* tissue engineering approaches, possibly by partly modifying the system or the device insertion.

In conclusion, this study first demonstrates that RB activated by ultrasound induces stiffening of porcine carotid arteries. Culturing of treated arteries leads to the induction of aneurysmal characteristics that are similar to the *in vivo* pathology. This model provides a promising tool to reduce *in vivo* animal experiments for studying aneurysm onset and progression and can be used for testing early stage devices or drugs.

References

Barton, M., Piller, S. C., Mahns, D. A. et al. (2012). In vitro cell compatibility study of rose bengal-chitosan adhesives. *Lasers Surg Med 44*, 762-768. doi:10.1002/lsm.22076

Bekesi, N., Gallego-Muñoz, P., Ibarés-Frías, L. et al. (2017). Biomechanical changes after in vivo collagen cross-linking with rose Bengal-green light and riboflavin-UVA. *Invest Ophthalmol Vis Sci 58*, 1612-1620. doi:10.1167/iovs.17-21475

Boekhoven, R. W., Rutten, M. C. M., van Sambeek, M. R. et al. (2014). Echo-computed tomography strain imaging of healthy and diseased carotid specimens. *Ultrasound Med Biol 40*, 1329-1342. doi:10.1016/j.ultrasmedbio.2013.11.026

Campa, J. S., Greenhalgh, R. M. and Powell, J. T. (1987). Elastin degradation in abdominal aortic aneurysms. *Atherosclerosis*, *65*, 13-21. doi:10.1016/0021-9150(87)90003-7

Carmo, M., Colombo, L., Bruno, A. et al. (2002). Alteration of elastin, collagen and their cross-links in abdominal aortic aneurysms. *Eur J Vasc Endovasc Surg 23*, 543-549. doi:10.1053/ejvs.2002.1620

Chen, X., Wang, J., Hou, J. et al. (2009). Extracellular matrix metalloproteinase inducer (EMMPRIN) is present in smooth muscle cells of human aneurysmal aorta and is induced by angiotensin II in vitro. *Clin Sci 116*, 819-826. doi:10.1042/CS20080235

Cherfan, D., Verter, E. E., Melki, S. et al. (2013). Collagen cross-linking using rose bengal and green light to increase corneal stiffness. *Invest Ophthalmol Vis Sci 54*, 3426-3433. doi:10.1167/iovs.12-11509

Czerski, A., Bujok, J., Gnus, J. et al. (2013). Experimental methods of abdominal aortic aneurysm creation in swine as a large animal model. *J Physiol Pharmacol 64*, 185-192.

Gandhi, R. H., Irizarry, E., Cantor, J. O. et al. (1994). Analysis of elastin cross-linking and the connective tissue matrix of abdominal aortic aneurysms. *Surgery 115*, 617-620.

García, A., Martínez, M. A. and Peña, E. (2012). Viscoelastic properties of the passive mechanical behavior of the porcine carotid artery: Influence of proximal and distal positions. *Biorheology 49*, 271-288. doi:10.3233/BIR-2012-0606

Gasser, T. C., Gallinetti, S., Xing, X. et al. (2012). Spatial orientation of collagen fibers in the abdominal aortic aneurysm's wall and its relation to wall mechanics. *Acta Biomater 8*, 3091-3103. doi:10.1016/j.actbio.2012.04.044

Giugliano, G., Gerardi, D., Annunziata, M. et al. (2018). Abdominal aortic aneurysm: Screening and management. *Continuing Cardiology Education 4*, 34-39. doi:10.1002/cce2.73

Golledge, J. and Norman, P. E. (2011). Current status of medical management for abdominal aortic aneurysm. *Atherosclerosis 217*, 57-63. doi:10.1016/j.atherosclerosis.2011.03.006

He, C. M. and Roach, M. R. (1994). The composition and mechanical properties of abdominal aortic aneurysms. *J Vasc Surg 20*, 6-13. doi:10.1016/0741-5214(94)90169-4

Hiraoka, W., Honda, H., Feril, L. B. et al. (2006). Comparison between sonodynamic effect and photodynamic effect with photosensitizers on free radical formation and cell killing. *Ultrason Sonochem 13*, 535-542. doi:10.1016/j.ultsonch.2005.10.001

Isenburg, J. C., Simionescu, D. T., Starcher, B. C. et al. (2007). Elastin stabilization for treatment of abdominal aortic aneurysms. *Circulation 115*, 1729-1737. doi:10.1161/circulationaha.106.672873

Johnston, K. W., Rutherford, R. B., Tilson, M. D. et al. (1991). Suggested standards for reporting on arterial aneurysms. *J Vasc Surg 13*, 452-458. doi:10.1067/mva.1991.26737

Lauto, A., Mawad, D., Barton, M. et al. (2010). Photochemical tissue bonding with chitosan adhesive films. *Biomed Eng Online 9*, 47. doi:10.1186/1475-925X-9-47

Li, J., Bao, X., Li, Y. et al. (2016). Study of the functional mechanisms of osteopontin and chemokine-like factor 1 in the development and progression of abdominal aortic aneurysms in rats. *Exp Ther Med 12*, 4007-4011. doi:10.3892/etm.2016.3891

Lindeman, J. H. N., Ashcroft, B. A., Beenakker, J. M. et al. (2010). Distinct defects in collagen microarchitecture underlie vessel-wall failure in advanced abdominal aneurysms and aneurysms in Marfan syndrome. *Proc Natl Acad Sci U S A 107*, 862-865. doi:10.1073/pnas.0910312107

Loizou, C. P., Pattichis, C. S., Nicolaides, A. N. et al. (2009). Manual and automated media and intima thickness measurements of the common carotid artery. *IEEE Trans Ultrason Ferroelectr Freg Control 56*, 983-994. doi:10.1109/TUFFC.2009.1130

Lysgaard Poulsen, J., Stubbe, J. and Lindholt, J. (2016). Animal models used to explore abdominal aortic aneurysms : A systematic review. *Eur J Vasc Endovasc Surg 52*, 487-499. doi:10.1016/j.ejvs.2016.07.004

MacSweeney, S. T. R., Young, Y., Greenhalgh, R. M. et al. (1992). Mechanical properties of the aneurysmal aorta. *Br J Surg 79*, 1281-1284. doi:10.1002/bjs.1800791211

Mao, N., Gu, T., Shi, E. et al. (2015). Phenotypic switching of vascular smooth muscle cells in animal model of rat thoracic aortic aneurysm. *Interact Cardiovasc Thorac Surg 21*, 62-70. doi:10.1093/icvts/ivv074

McGee, G. S., Baxter, B. T., Shively, V. P. et al. (1991). Aneurysm or occlusive disease – Factors determining the clinical course of atherosclerosis of the infrarenal aorta. *Surgery 110*, 370-376.

Nakonechny, F., Nisnevitch, M., Nitzan, Y. et al. (2013). Sonodynamic excitation of Rose Bengal for eradication of gram-positive and gram-negative bacteria. *Biomed Res Int 2013*, 684930. doi:10.1155/2013/684930

Nordon, I. M., Hinchliffe, R. J., Loftus, I. M. et al. (2011). Pathophysiology and epidemiology of abdominal aortic aneurysms. *Nat Rev Cardiol 8*, 92-102. doi:10.1038/nrcardio.2010.180

Nuki, Y., Tsou, T.-L., Kurihara, C. et al. (2009). Elastase-induced intracranial aneurysms in hypertensive mice. *Hypertension 54*, 1337-1344. doi:10.1161/hypertensionaha.109.138297

O'Neill, A. C., Winograd, J. M., Zeballos, J. L. et al. (2007). Microvascular anastomosis using a photochemical tissue bonding technique. *Lasers Surg Med 39*, 716-722. doi:10.1002/lsm.20548

Patelis, N., Moris, D., Schizas, D. et al. (2017). Animal models in the research of abdominal aortic aneurysms development. *Physiol Res 66*, 899-915.

Ren, W., Liu, Y., Wang, X. et al. (2016). β-Aminopropionitrile monofumarate induces thoracic aortic dissection in C57BL/6 mice. *Sci Rep 6*, 1-7. doi:10.1038/srep28149

Riches, K., Angelini, T. G., Mudhar, G. S. et al. (2013). Exploring smooth muscle phenotype and function in a bioreactor model of abdominal aortic aneurysm. *J Transl Med 11*, 208. doi:10.1186/1479-5876-11-208

Rizzo, R. J., McCarthy, W. J., Dixit, S. N. et al. (1989). Collagen types and matrix protein content in human abdominal aortic aneurysms. *J Vasc Surg 10*, 365-373. doi:10.1016/0741-5214(89)90409-6

Robertson, A. R., Duan, X., Aziz, K. M. et al. (2015). Diversity in the strength and structure of unruptured cerebral aneurysms. *Ann Biomed Eng 43*, 1502-1515. doi:10.1007/s10439-015-1252-4

Roy, S., Silacci, P. and Stergiopulos, N. (2005). Biomechanical properties of decellularized porcine common carotid arteries. *Am J Physiol Heart Circ Physiol 289*, 1567-1576. doi:10.1152/ajpheart.00564.2004

Salinas, H. M., Khan, S. I., McCormack, M. C. et al. (2017). Prevention of vein graft intimal hyperplasia with photochemical tissue passivation. *J Vasc Surg 65*, 190-196. doi:10.1016/j.jvs.2015.11.049

Sokolis, D. P., Sassani, S., Kritharis, E. P. et al. (2011). Differential histomechanical response of carotid artery in relation to species and region: Mathematical description accounting for elastin and collagen anisotropy. *Med Biol Eng Comput 49*, 867-879. doi:10.1007/s11517-011-0784-5

Sonesson, B., Hansen, F. and Lanne, T. (1997). Abdominal aortic aneurysm: A general defect in the vasculature with focal manifestations in the abdominal aorta? *J Vasc Surg 26*, 247-254. doi:10.1016/S0741-5214(97)70185-X

Tanweer, O., Wilson, T. A., Metaxa, E. et al. (2014). A comparative review of the hemodynamics and pathogenesis of cerebral and abdominal aortic aneurysms: Lessons to learn from each other. *J Cerebrovasc Endovasc Neurosurg 16*, 335-349. doi:10.1136/neurintsurg-2014-011343.83

Touroo, J. S. and Williams, S. K. (2012). A tissue-engineered aneurysm model for evaluation of endovascular devices. *J Biomed Mater Res A 100*, 3189-3196. doi:10.1002/jbm.a.34256

Trachet, B., Piersigilli, A., Fraga-Silva, R. A. et al. (2016). Ascending aortic aneurysm in angiotensin II-infused mice: Formation, progression, and the role of focal dissections. *Arterioscler Thromb Vasc Biol 36*, 673-681. doi:10.1161/atvbaha.116.307211

Upchurch, G. R. and Criado, E. (eds.) (2009). Aortic aneurysms – Pathogenesis and treatment. In *Contemporary Cardiology – Book Series*. Humana Press. doi:10.1007/978-1-60327-204-9

Vande Geest, J. P., Sacks, M. S. and Vorp, D. A. (2006). The effects of aneurysm on the biaxial mechanical behavior of human abdominal aorta. *J Biomech 39*, 1324-1334. doi:10.1016/j.jbiomech.2005.03.003

Vanerio, N., Stijnen, M., de Mol, B. A. and Kock, L. M. (2019a). An innovative ex vivo vascular bioreactor as comprehensive tool to study the behavior of native blood vessels under physiologically relevant conditions. *ASME J of Medical Diagnostics 2*, 041003. doi:10.1115/1.4044472

Vanerio, N., Stijnen, M., de Mol, B. A. and Kock, L. M. (2019b). Biomedical applications of photo- and sono-activated Rose Bengal: A review. *Photobiomodul Photomed Laser Surg 37*, 383-394. doi:10.1089/photob.2018.4604

Wågsäter, D., Paloschi, V., Hanemaaijer, R. et al. (2013). Impaired collagen biosynthesis and cross-linking in aorta of patients with bicuspid aortic valve. *J Am Heart Assoc 2*, e000034. doi:10.1161/JAHA.112.000034

Xu, N., Yao, M., Farinelli, W. A. et al. (2015). Light-activated sealing of skin wounds. *Lasers Surg Med 47*, 17-29. doi:10.1002/lsm.22308

Conflict of interest

Noemi Vanerio, Marco Stijnen and Linda M. Kock are employees of LifeTec Group BV. Bas A. J. M. de Mol is an advisor of LifeTec Group BV.

Acknowledgements

This work was supported by the European Commission within the Horizon 2020 Framework through the MSCA-ITN-ETN European Training Networks (project number 642458).